Title

Accurate T1 mapping of short T2 tissues using a three-dimensional ultrashort echo time cones actual flip angle imaging-variable repetition time (3D UTE-Cones AFI-VTR) method

Journal

Magnetic Resonance in Medicine, 80(2)

ISSN

0740-3194

Authors

Ma, Ya-Jun
Lu, Xing
Carl, Michael
et al.

Publication Date

2018-08-01

DOI

10.1002/mrm.27066

Peer reviewed

Accurate T_1 Mapping of Short T_2 Tissues Using a Three-Dimensional Ultrashort Echo Time Cones Actual Flip Angle Imaging-Variable Repetition Time (3D UTE-Cones AFI-VTR) Method

Ya-Jun Ma,[1] Xing Lu,[1] Michael Carl,[2] Yanchun Zhu,[1] Nikolaus M. Szeverenyi,[1] Graeme M. Bydder,[1] Eric Y. Chang,[1,3] and Jiang Du[1]*

Purpose: To develop an accurate T_1 measurement method for short T_2 tissues using a combination of a 3-dimensional ultrashort echo time cones actual flip angle imaging technique and a variable repetition time technique (3D UTE-Cones AFI-VTR) on a clinical 3T scanner.

Methods: First, the longitudinal magnetization mapping function of the excitation pulse was obtained with the 3D UTE-Cones AFI method, which provided information about excitation efficiency and B_1 inhomogeneity. Then, the derived mapping function was substituted into the VTR fitting to generate accurate T_1 maps. Numerical simulation and phantom studies were carried out to compare the AFI-VTR method with a B_1-uncorrected VTR method, a B_1-uncorrected variable flip angle (VFA) method, and a B_1-corrected VFA method. Finally, the 3D UTE-Cones AFI-VTR method was applied to bovine bone samples ($N = 6$) and healthy volunteers ($N = 3$) to quantify the T_1 of cortical bone.

Results: Numerical simulation and phantom studies showed that the 3D UTE-Cones AFI-VTR technique provides more accurate measurement of the T_1 of short T_2 tissues than the B_1-uncorrected VTR and VFA methods or the B_1-corrected VFA method. The proposed 3D UTE-Cones AFI-VTR method showed a mean T_1 of 240 ± 25 ms for bovine cortical bone and 218 ± 10 ms for the tibial midshaft of human volunteers, respectively, at 3 T.

Conclusion: The 3D UTE-Cones AFI-VTR method can provide accurate T_1 measurements of short T_2 tissues such as cortical bone. **Magn Reson Med 80:598–608, 2018. © 2018 International Society for Magnetic Resonance in Medicine.**

Key words: ultrashort echo time; actual flip angle imaging; variable TR; cortical bone

INTRODUCTION

Variable flip angle (VFA) and variable repetition time (VTR) methods based on 3-dimensional (3D) spoiled gradient recalled echo (SPGR) sequences have been used widely for volumetric T_1 measurement (1–5). However, both the VFA and VTR methods are very sensitive to inhomogeneity in the transmitted B_1 field. As a result, the first step for accurate T_1 measurement usually requires obtaining spatial B_1 field maps (6–15). These are then used for accurate T_1 calculation (16–21).

The actual flip angle imaging (AFI) technique has been proposed for fast 3D B_1 mapping (15). It uses interleaved acquisitions of dual repetition-time (TR) steady-state signals that are formed by alternately changing the TR of a conventional SPGR sequence. The robustness of the AFI technique has been demonstrated for mapping the B_1 of long T_2 tissues of the human body (15,20,21). However, the typical AFI sequence cannot be used for mapping the B_1 of short T_2 tissues, such as cortical bone, calcified cartilage, menisci, ligaments, and tendons (18,19). This is because these tissues have short T_2 values ranging from several hundred microseconds to a few milliseconds, and show little or no signal when imaged with conventional SPGR sequences that have echo times (TEs) of several milliseconds. Ultrashort echo time (UTE) sequences with TEs less than 100 μs have been developed for imaging of short T_2 tissues, and produce detectable signals (4,22,23). Combination of the UTE and AFI techniques (UTE-AFI) would therefore appear to be an appropriate way to map flip angles for short T_2 tissues (18,19).

However, there are technical challenges in accurately mapping flip angles when imaging short T_2 tissues such as cortical bone, because of transverse relaxation during the radiofrequency (RF) excitation pulse. This is typically ignored for long T_2 tissues, but becomes significant when imaging short T_2 tissues. Large flip angles ($>40°$) are typically required to make the AFI technique sensitive (15,18). With conventional peak power limitations on the RF amplifiers of clinical scanners, the RF pulse duration must be increased to produce such large flip angle excitations. However, excitation efficiency is decreased when imaging short T_2 tissues with longer RF excitation pulses, as a result of transverse relaxation during the pulse, and this leads to actual flip angles that are lower than the nominal flip angles (i.e., the expected flip angles) (23–26). This causes B_1 estimation errors when the UTE-AFI method is used for imaging short T_2 tissues (as detailed in the "Theory" section). It can result in inaccurate T_1 values for short T_2 tissues.

[1]Department of Radiology, University of California, San Diego, California, USA.
[2]GE Healthcare, San Diego, California, USA.
[3]Radiology Service, VA San Diego Healthcare System, San Diego, California, USA.
*Correspondence to: Jiang Du, Ph.D., Department of Radiology, University of California, San Diego, 200 West Arbor Drive, San Diego, CA 92103-8226, USA. E-mail: jiangdu@ucsd.edu

Grant Support: GE Healthcare, NIH (1R01 AR062581 and 1R01 AR068987), and the VA Clinical Science Research & Development Service (1I01CX001388).
Received 11 September 2017; revised 14 November 2017; accepted 11 December 2017
DOI 10.1002/mrm.27066
Published online 3 January 2018 in Wiley Online Library (wileyonlinelibrary.com).

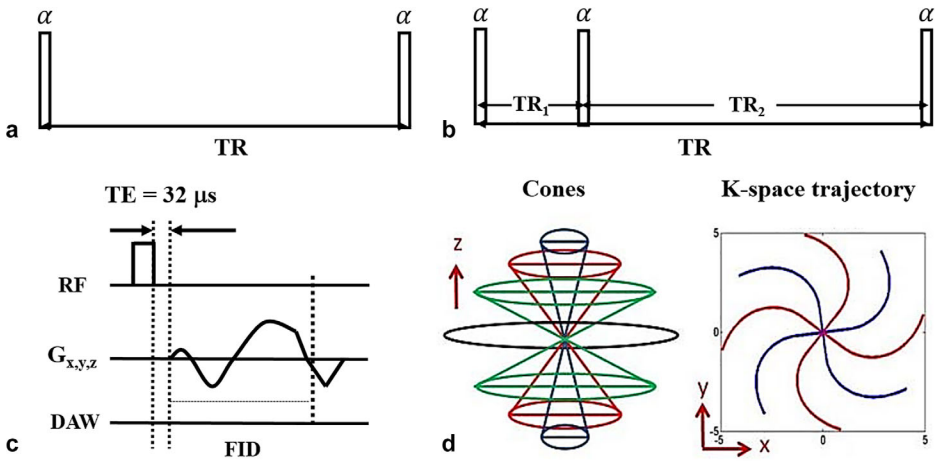

FIG. 1. **a**: Conventional 3-dimensional ultrashort echo time cones (3D UTE-Cones) sequence with a single repetition time (TR) is used for T_1 measurement with the variable flip angle (VFA) or variable TR (VTR) method. The 3D UTE-Cones actual flip angle imaging (AFI) sequence uses a pair of interleaved TRs for accurate B_1 mapping (**b**), which together with a VFA or VTR method provides T_1 measurements. In these two UTE-Cones sequences, a short rectangular pulse is used for signal excitation followed by 3D spiral sampling with a very short TE of 32 μs (**c**). The spiral trajectories are arranged with conical view ordering (**d**). RF, radiofrequency; DAW, data acquisition window.

To overcome this problem, we propose a new T_1 measurement method for short T_2 tissues that combines a 3D UTE-Cones AFI technique with a 3D UTE-Cones VTR technique (3D UTE-Cones AFI-VTR). In this method, the same RF pulses and flip angles are used for signal excitation in the AFI and VTR sequences. As a result, B_1 maps are no longer required for T_1 correction. Instead, the longitudinal magnetization mapping function of the RF excitation pulse is obtained by the 3D UTE-Cones AFI method, and this is subsequently used for VTR-based T_1 fitting. Simulation, phantom, and in vivo studies were used to investigate the accuracy of the proposed method for measuring the T_1 of cortical bone, using parameters that are appropriate for a clinical 3T scanner.

THEORY

Features of the conventional 3D UTE-Cones pulse sequence with a single TR (Fig. 1a) have been described before (27–29). Actual flip angle imaging can be achieved with the 3D dual TR UTE-Cones sequence (Fig. 1b). A series of conventional 3D UTE-Cones sequences with variable TRs or variable flip angles can then be used for T_1 measurement. For both the UTE-Cones AFI and the UTE-Cones VTR/VFA sequences, a short rectangular pulse (e.g., 150 μs) was used for nonselective signal excitation (Fig. 1c). This was followed by a spiral trajectory data acquisition with conical view ordering (Fig. 1d).

The steady-state signals acquired in TR_1 and TR_2 of the 3D UTE-Cones AFI sequence can be expressed as follows (15,25):

$$S_1 = M_0 f_{xy}(\alpha,\tau,T_2)\frac{1-E_2+(1-E_1)E_2 f_z(\alpha,\tau,T_2)}{1-E_1E_2f_z^2(\alpha,\tau,T_2)} \quad [1]$$

$$S_2 = M_0 f_{xy}(\alpha,\tau,T_2)\frac{1-E_1+(1-E_2)E_1 f_z(\alpha,\tau,T_2)}{1-E_1E_2f_z^2(\alpha,\tau,T_2)} \quad [2]$$

where $E_1 = \exp(-TR_1/T_1)$ and $E_2 = \exp(-TR_2/T_1)$; M_0 is the equilibrium magnetization; $f_{xy}(\alpha,\tau,T_2)$ and $f_z(\alpha,\tau,T_2)$ are the respective transverse and longitudinal magnetization mapping functions generated by the RF pulse, with $f_{xy}(\alpha,\tau,T_2) = M_{xy}^+/M_z^-$ and $f_z(\alpha,\tau,T_2) = M_z^+/M_z^-$.; M_z^- is the longitudinal magnetization before RF excitation; M_{xy}^+ and M_z^+ are the transverse and longitudinal magnetizations after the RF excitation; α is the flip angle; and τ is the duration of the rectangular excitation pulse. Because the RF pulse duration is much shorter than the tissue T_1, T_1 relaxation during the excitation can be neglected in the mapping functions.

For short T_2 tissues with T_2 values of the same order as the RF duration τ, $f_{xy}(\alpha,\tau,T_2)$ and $f_z(\alpha,\tau,T_2)$ are determined not only by α, but also by τ and the tissue T_2. Analytical expressions of these two terms can be described as follows (24):

$$f_{xy}(\alpha,\tau,T_2) = e^{-\frac{\tau}{2T_2}}\alpha\,\mathrm{sinc}\left(\sqrt{\alpha^2-\left(\frac{\tau}{2T_2}\right)^2}\right) \quad [3]$$

$$f_z(\alpha,\tau,T_2) = e^{-\frac{\tau}{2T_2}}\left(cos\left(\sqrt{\alpha^2-\left(\frac{\tau}{2T_2}\right)^2}\right) + \frac{\tau}{2T_2}\mathrm{sinc}\left(\sqrt{\alpha^2-\left(\frac{\tau}{2T_2}\right)^2}\right)\right) \quad [4]$$

For long T_2 tissues with T_2s $\gg$ τ, $f_{xy}(\alpha,\tau,T_2)$ and $f_z(\alpha,\tau,T_2)$, simplify to sin(α) and cos(α), respectively. Equations [1] and [2] then become identical to the conventional expression for AFI in Equation [3] as shown in (30).

The general AFI method relies on two fundamental assumptions: (i) that complete spoiling of the transverse magnetization occurs during TR_1 and TR_2; and (ii) that TR_1s and TR_2s are short compared with T_1. Perfect spoiling during each TR is very difficult to achieve, as high flip angles and relatively short TRs are used in AFI (15).

Yarnykh suggested the use of an optimized combination of RF spoiling with an extremely strong gradient crusher pair to provide additional spoiling (17). However, in this study the heavy gradient spoiler and phase cycling to provide RF spoiling may not be necessary for complete spoiling, because of the fast decay of the transverse magnetization of short T_2 tissues. With TRs that are short relative to T_1, the signal ratio r of S_1 and S_2 can be simplified using a first-order approximation for the exponential terms such that (15)

$$r = S_2/S_1 \approx \frac{1 + nf_z(\alpha, \tau, T_2)}{n + f_z(\alpha, \tau, T_2)} \quad [5]$$

where $n = TR_2/TR_1$. The ratio r can then be used as a T_1-independent measure of $f_z(\alpha, \tau, T_2)$:

$$f_z(\alpha, \tau, T_2) \approx \frac{rn - 1}{n - r} \quad [6]$$

For long T_2 tissues, $f_z(\alpha, \tau, T_2)$ becomes cos(α). Therefore, the actual flip angle α can be estimated with the following equation (15):

$$\alpha \approx arc\ \cos\left(\frac{rn - 1}{n - r}\right) \quad [7]$$

Then, the B_1 scaling factor (B_{1s}) is obtained by dividing the measured α by the nominal flip angle α_{nom}, which is expressed as

$$B_{1s} = \alpha/\alpha_{nom} \quad [8]$$

where B_{1s} is used to quantify the RF inhomogeneity, and $B_{1s} = 1$ corresponds to an unaltered RF field.

For short T_2 tissues, the measurement of α or B_{1s} is more complicated. With knowledge of the RF pulse duration and tissue T_2, α can be calculated from the analytical expression for $f_z(\alpha, \tau, T_2)$ or through Bloch equation simulation. However, it is very challenging to measure short T_2 values using the traditional spin echo or Carr-Purcell-Meiboom-Gill method, because of the rapid tissue signal decay as well as the limited RF peak power and gradient strength available on clinical MR scanners. Furthermore, these methods may require extra sequences to measure short T_2 values, which subsequently suffer from errors caused by magnetization transfer (when the 2D multislice spin-echo or the Carr-Purcell-Meiboom-Gill sequence is used to measure T_2), potential motion artifacts associated with the increased scan time, and limited signal-to-noise ratio when imaging short T_2 tissues. To cope with these issues, we propose a new approach that avoids the calculation of α required in standard approaches. The value of $f_z(\alpha, \tau, T_2)$ is used directly as input for T_1 calculation under the VTR method. The description of our method follows.

The 3D UTE-Cones sequence is a free induction decay sequence characterized by an ultrashort TE ($TE = 32\,\mu s$) and a 3D non-Cartesian center-out k-space encoding scheme. The detected magnetization S_{spgr} follows the same steady-state behavior as the signal acquired with a SPGR sequence and is expressed as follows (25,30):

$$S_{spgr} = M_0 f_{xy,s}(\alpha, \tau, T_2) \frac{1 - E}{1 - Ef_{z,s}(\alpha, \tau, T_2)} \quad [9]$$

with $E = exp(-TR_s/T_1)$where TR_s is the repetition time (TR) of the UTE-Cones sequence; and $f_{xy,s}(\alpha, \tau, T_2)$ and $f_{z,s}(\alpha, \tau, T_2)$ are the RF pulse–induced transverse and longitudinal mapping functions, respectively. Analogous to $f_{xy}(\alpha, \tau, T_2)$ and $f_z(\alpha, \tau, T_2)$ in Equations [1] and [2], $f_{xy,s}(\alpha, \tau, T_2)$ and $f_{z,s}(\alpha, \tau, T_2)$ become sin(α) and cos(α) for long T_2 tissues.

Fitting of Equation [9] can be used for T_1 quantification of short T_2 tissues from VTR or VFA UTE-Cones data. For long T_2 tissues, the VTR and VFA data are processed with the actual flip angles, which can be calculated by applying the B_1 scaling factor B_{1s} to the nominal flip angles. Because it is complicated to measure B_{1s} for short T_2 tissues, we propose a new T_1 measurement technique that combines the UTE-AFI method and the UTE VTR method, and uses identical RF excitation pulses. As a result, $f_{z,s}(\alpha, \tau, T_2)$ in Equation [9] is identical to $f_z(\alpha, \tau, T_2)$ in Equation [6]. In the T_1 fitting procedure with the VTR method, the coefficients M_0 and $f_{xy,s}(\alpha, \tau, T_2)$ in Equation [9] can be combined into a single unknown parameter (e.g., g), as M_0 and $f_{xy,s}(\alpha, \tau, T_2)$ are both not functions of TR. After the measured $f_z(\alpha, \tau, T_2)$ from Equation [6] is substituted into Equation [9], there are only two unknown parameters including g and T_1. Therefore, robust T_1 measurements can be achieved by fitting the data with variable TRs.

METHODS

In our study, the 3D UTE-Cones AFI and conventional UTE-Cones sequences (Fig. 1) were implemented on a 3T Signa TwinSpeed scanner (GE Healthcare Technologies, Milwaukee, WI, USA). An eight-channel transmit/receive knee coil was used for both RF transmission and signal reception. The sequences used unique k-space trajectories that sampled data along evenly spaced twisted paths in the form of multiple cones (27–29). Data sampling began from the center of k-space and continued outward. It began as soon as practical after the RF excitation with a minimal nominal delay time of 32 μs. Both RF and gradient spoiling were used to crush the remaining transverse magnetizations. In 3D UTE-Cones AFI, the areas of gradient crushers in TR_1 and TR_2 were 180 and 900 mT· ms/m, respectively, and the RF phase increment was 39° 39° (17). In 3D VTR or VFA UTE-Cones, the area of the gradient crushers was 180 mT· ms/m, and the RF phase increment was 169° 169° (17). The 3D UTE-Cones sequence allowed anisotropic resolution (e.g., high in-plane resolution and thicker slices) to provide an improved signal-to-noise ratio and a reduced scan time relative to isotropic imaging (28,29).

Simulation

Numerical simulation was performed to investigate the accuracy of the proposed T_1 measurement for short T_2 tissues. Identical simulated rectangular RF pulses were used for signal excitation in both the 3D UTE-Cones AFI and VTR sequences, and had durations from 0.1 to 500 μs. T_2 values of simulated short T_2 tissues ranged

Table 1
Sequence Parameters of Phantom, Bovine Cortical Bone Sample, and In Vivo Tibial Cortical Bone Studies

	3D UTE-Cones AFI	3D UTE-Cones VTR	3D UTE-Cones VFA
Phantom	FOV = 15 × 15 × 12.8 cm^3, matrix = 128 × 128 × 32, TR_1/TR_2 = 20/100 ms, flip angle = 45°, bandwidth = 125 kHz, scan time = 8 min 55 s	FOV = 15 × 15 × 12.8 cm^3, matrix = 128 × 128 × 32, TR = 20, 40, 60, 80 and 120 ms, flip angle = 45°, bandwidth = 125 kHz, total scan time = 21 min 20 s	FOV = 15 × 15 × 12.8 cm^3, matrix = 128 × 128 × 32, TR = 24 ms, flip angle = 8°, 26° and 45°, bandwidth = 125 kHz, total scan time = 5 min 21 s
	3D UTE-Cones AFI	3D UTE-Cones VTR	
Bovine cortical bone	FOV = 15 × 15 × 6.4 cm^3, matrix = 128 × 128 × 16, TR_1/TR_2 = 20/100 ms, flip angle = 45°, bandwidth = 125 kHz, scan time = 4 min 40 s	FOV = 15 × 15 × 6.4 cm^3, matrix = 128 × 128 × 16, TR = 15, 30, 50 and 80 ms, bandwidth = 125 kHz, total scan time = 6 min 41 s	
	3D UTE-Cones AFI	3D UTE-Cones VTR	
In vivo tibial cortical bone	FOV = 15 × 15 × 16.8 cm^3, matrix = 128 × 128 × 24, TR_1/TR_2 = 20/100 ms, flip angle = 45°, bandwidth = 250 kHz, scan time = 7 min 5 s	FOV = 15 × 15 × 16.8 cm^3, matrix = 160 × 160 × 24, TR = 15, 30, 50 and 80 ms, flip angle = 45°, bandwidth = 250 kHz, total scan time = 12 min 24 s	

Note: FOV, field of view.

from 0 to 1 ms. The T_1 value was set to 500 ms. The sequence parameters for the 3D UTE-Cones AFI and VTR sequences were adjusted as follows: (i) 3D UTE-Cones AFI: TR_1/TR_2 = 20/100 ms and flip angle = 45°; (ii) VTR UTE-Cones: TR = 10, 50, 100, 150, and 200 ms, and flip angle = 45°. For comparison, the VFA UTE-Cones sequence was also used for T_1 measurement with the following sequence parameters: TR = 20 ms and flip angles = 7°, 14°, 22°, 30°, and 38° (31). Three simulated nominal B_1 scaling factors (B_{1n}) were used and set to values of 0.8, 1, and 1.2.

Phantom and Sample Study

An agarose phantom was prepared by adding 3.0 g agarose powder and 7.2 mg $MnCl_2 \cdot 4H_2O$ to 400 mL distilled water. The mixture was brought to a boil in a microwave oven and then cooled in a refrigerator, allowing the solution to gel. The T_2 value of the agarose phantom was approximately 80 ms. This was designed to simulate long T_2 tissue. Another agarose phantom was prepared by mixing 300 mL distilled water with the same concentrations of agarose and $MnCl_2$ as in the previous phantom. After bringing the solution to a boil, the solution was cooled to 40°, and a fresh bovine cortical bone section that had been stripped of soft tissue was suspended within it. The phantom was then allowed to cool until the agarose gelled with the suspended bone section immobilized within it. In addition, five fresh bovine cortical bone sections were stripped of soft tissue and submerged in Fomblin (perfluoropolyether) within a cylindrical container of suitable size for MR scanning. These phantoms were scanned with the 3D UTE-Cones AFI, VTR and VFA sequences, and the sequence parameters can be found in Table 1.

A bovine cortical bone sample was used to compare the two VTR T_1 measurement techniques using two different excitation flip angles of 20° and 45° with RF pulse durations of 60 and 150 μs, respectively. The power of the RF pulses was near the maximum available on the clinical scanner. The UTE-Cones AFI method was used to obtain the mapping function magnetization, $f_z(\alpha, \tau, T_2)$, which was subsequently used to correct T_1 measurement errors induced by both B_1 inhomogeneity and loss of magnetization during the 45° excitation pulse. The 20° pulse with a duration of 60 μs was more effective than the 45° pulse in generating transverse magnetization for materials with short T_2s, as the pulse duration was much shorter than the typical T_2^* value for bovine cortical bone, which is approximately 300 μs (4). The error in T_1 measurement with a 20° pulse was expected to come primarily from B_1 inhomogeneity. Other sequence parameters can be found in Table 1.

Another bovine cortical bone sample was used to investigate the T_1 measurement accuracy of the proposed 3D UTE-Cones AFI-VTR method using three different RF pulse durations of 150, 200, and 300 μs with the same flip angle of 45°. Identical excitation pulses were used for the UTE-Cones AFI and VTR sequences. The AFI and VTR sequences were each scanned three times using the RF excitation pulses of different duration mentioned previously. Other sequence parameters were identical to the above bovine cortical bone study.

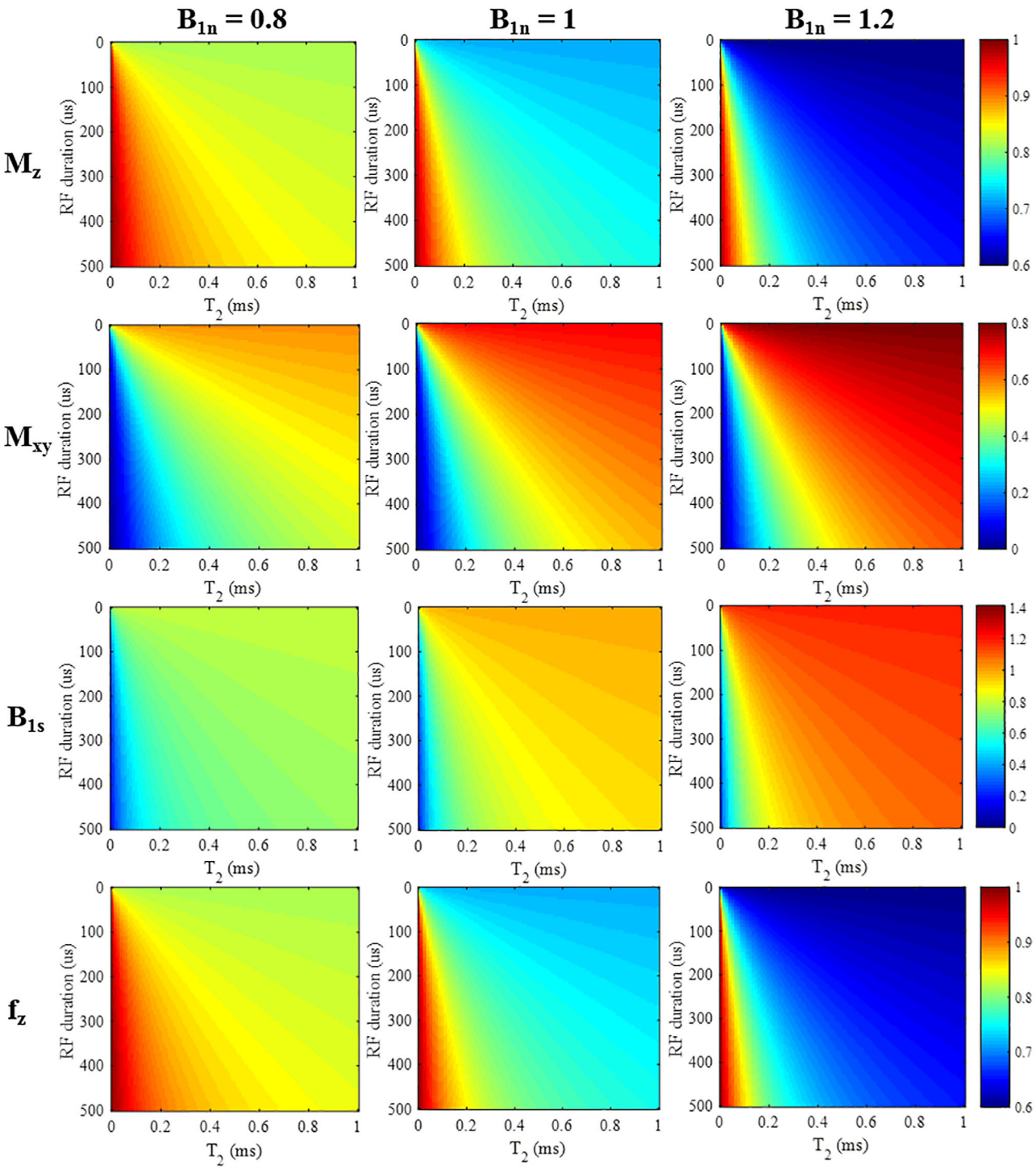

FIG. 2. Simulation results for short T_2 tissues (T_2s from 0 to 1 ms) with a rectangular RF pulse excitation (durations from 0.1 to 500 μs). The top two rows show color maps corresponding to the longitudinal and transverse magnetizations (i.e., $f_z(\alpha,\tau,T_2)$ and $f_{xy}(\alpha,\tau,T_2)$), calculated from Equations [3] and [4]. The third row shows the resulting B_{1s} scaling factors, and the bottom row shows the mapping function $f_z(\alpha,\tau,T_2)$ obtained by the AFI method. The columns represent simulation results with nominal B_1 scaling factors B_{1n} of 0.8, 1, and 1.2, respectively.

In Vivo Study

The 3D UTE-Cones AFI-VTR method was tested in vivo on three healthy male volunteers (ages 29, 35, and 40 years). Informed consent was obtained from all subjects in accordance with local institutional review board guidelines. Sequence parameters can be found in Table 1. A higher bandwidth was used for in vivo imaging of cortical bone to minimize chemical shift artifacts from bone marrow fat, which are manifest as ring-shaped artifacts with 3D UTE-Cones imaging.

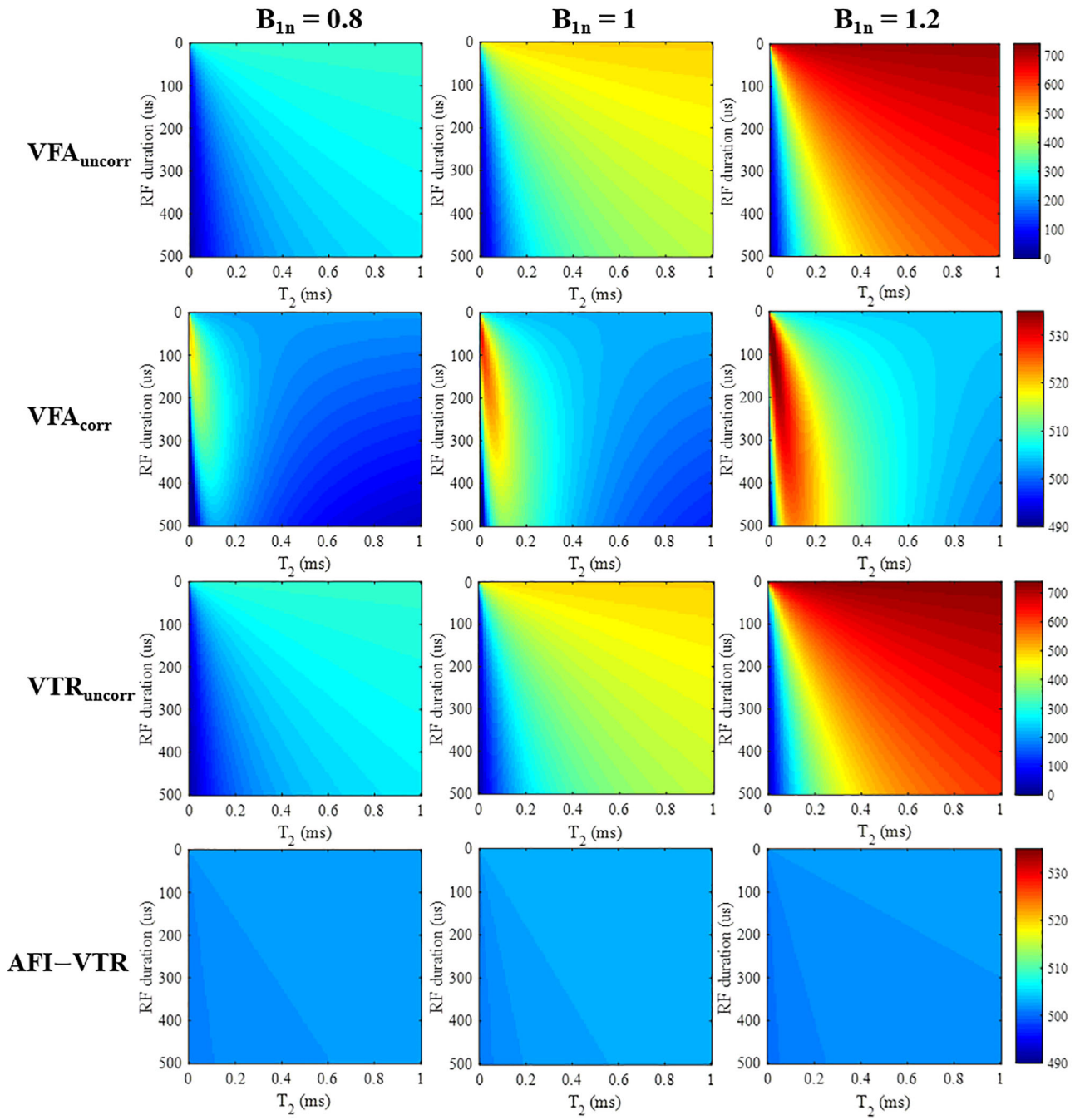

FIG. 3. T_1 mapping results (in units of ms) generated by the VFA method without (first row) and with (second row) B_1 correction, as well as results using the VTR method without (third row) and with (fourth row) B_1 correction. The columns show simulation results with nominal B_1 scaling factors B_{1n} of 0.8, 1, and 1.2, respectively. The AFI-VTR method provides the most consistent T_1 values over the range of short T_2 tissues (T_2s from 0 to 1 ms).

Data Analysis

The Levenberg-Marquardt algorithm in MATLAB (The MathWorks Inc, Natick, MA, USA) was used to solve the nonlinear fitting of Equation [9] for both VTR and VFA methods. The analysis algorithms written in MATLAB were applied to the DICOM images obtained from the 3D UTE-Cones AFI and VTR/VFA UTE-Cones protocols described previously. After each fitting calculation, B_{1s} scaling factor $f_z(\alpha, \tau, T_2)$ and T_1 maps were generated. The mean value and standard deviation of T_1 for both in vitro bovine cortical bone ($N = 6$) and in vivo human tibial midshaft cortical bone ($N = 3$) were also calculated.

RESULTS

Figure 2 shows the simulation results. The top two rows show the theoretical longitudinal (M_z) and transverse (M_{xy}) magnetizations generated by the rectangular RF pulses with variable durations for a variety of short T_2s. In actual scanning, M_z and observed M_{xy} magnetizations correspond to $f_z(\alpha, \tau, T_2)$ and $f_{xy}(\alpha, \tau, T_2)$, which were

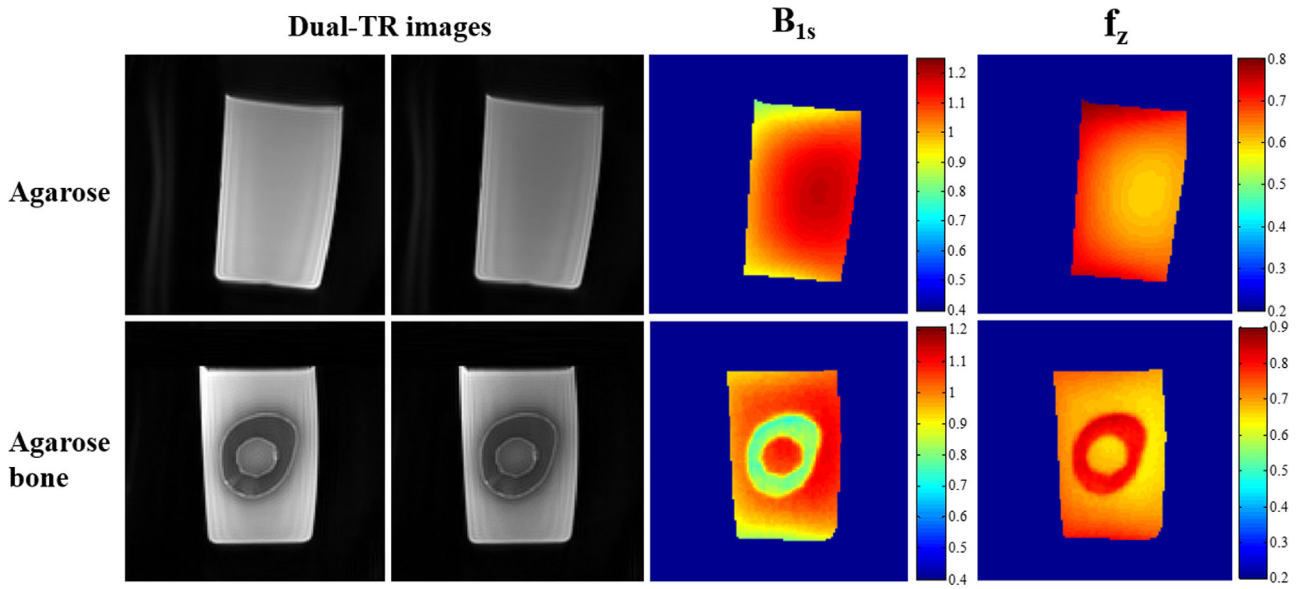

FIG. 4. Phantom results using the 3D UTE-Cones-AFI technique and an eight-channel knee coil. The first two columns show dual-TR UTE-Cones images (left: first TR images; right: second TR images) of an agarose phantom and an agarose bone phantom, whose B_{1s} and f_z maps are shown in the right two columns, respectively. As shown from the results of agarose phantom, higher B_{1s} is observed in the center area of the knee coil. However, the bone region in the agarose bone B_{1s} map shows much-reduced B_{1s} values as a result of inefficient excitation of the short T_2 tissue.

obtained using Equations [3] and [4]. From the color maps (Fig. 2), it can be seen that longer RF pulses are less effective than shorter pulses in generating M_{xy} for shorter T_2 tissue components. As expected, more M_{xy} is generated when the excitation pulse power is increased (i.e., when the nominal B_1 scaling factor B_{1n} is increased from 0.8 to 1.2). The bottom two rows in Figure 2 provide the estimated B_1 scaling factors B_{1s} and $f_z(\alpha, \tau, T_2)$, computed using the AFI method with Equations [8] and [6]. The measured B_1 scaling factors B_{1s} are more accurate when using shorter RF pulses and when imaging longer T_2 species. Otherwise, the estimated B_1 scaling factors B_{1s} are smaller than the nominal values. The calculated values of $f_z(\alpha, \tau, T_2)$ were nearly identical to the theoretical values of $f_z(\alpha, \tau, T_2)$ (i.e., M_z shown in the first row), which demonstrates the accuracy of Equation [6].

Figure 3 presents the simulation results of T_1 measurements using both VFA and VTR methods, with and without AFI correction. As seen in the bottom-left corners of all images in the first and third rows, T_1s from B_1-uncorrected VFA and VTR methods are both subject to underestimation caused by the imperfect excitation when using a longer RF pulse or when imaging shorter T_2 species. Additionally, the estimated T_1 values increase with larger values of the nominal B_1 scaling factor B_{1n}. The second row presents the VFA results using the conventional B_1 correction method (appropriate for long T_2 tissues). The calculated B_{1s} maps used for correction are displayed in the third row of Figure 3. Overall, the B_1-corrected VFA method is more accurate than the B_1-uncorrected VFA method. However, T_1 estimation errors still exist—especially for tissues with T_2s shorter than 0.5 ms, and the errors become larger with increased B_1 inhomogeneity. In contrast, the proposed AFI-VTR T_1 measurements presented in the last row are nearly accurate for all short T_2s, independent of the duration of the excitation pulses. Additionally, identical T_1 values are obtained with different values of the nominal B_1 scaling factor B_{1n}. The proposed AFI-VTR T_1 measurement method can eliminate errors induced by B_1 inhomogeneity, and is also immune to the imperfect signal excitation encountered with short T_2 species.

Figure 4 shows the phantom results obtained using the UTE-Cones AFI method. A smooth, continuous spatial distribution is observed in the agarose phantom maps, corresponding to the measured B_1 inhomogeneity (calculated from Eqs. [7] and [8]) and $f_z(\alpha, \tau, T_2)$ distribution (calculated from Eq. [6]). High flip angles tend to appear in the central region of the knee coil. Similar results are seen in the pure agarose region of the agarose bone phantom. There are clear sharp boundaries between the bone and agarose regions in both the B_{1s} and $f_z(\alpha, \tau, T_2)$ maps. The measured B_{1s} values in the bone region are lower than those in the agarose region as a result of inefficient excitation of cortical bone with its extremely short T_2. The experimental results agree well with the simulation results presented in Figure 2. The sharp discontinuities in the B_{1s} map suggest that the B_1 measurement is inaccurate for cortical bone, whereas the $f_z(\alpha, \tau, T_2)$ values in the bone region are reasonable and consistent.

Figure 5 demonstrates the effect of short tissue T_2s on the T_1 map calculation. Figures 5a and 5b show the regions of interest (ROIs) extracted from Figures 4e and 4f, which show the spatial distribution of B_{1s} and $f_z(\alpha, \tau, T_2)$. B_1 inhomogeneity and excitation inefficiency lead to complicated distributions in the bone region of the agarose-suspended bone phantom. The VFA T_1 map in the bone region still suffers from signal inhomogeneity, even with B_1 correction. The bone T_1 map measured

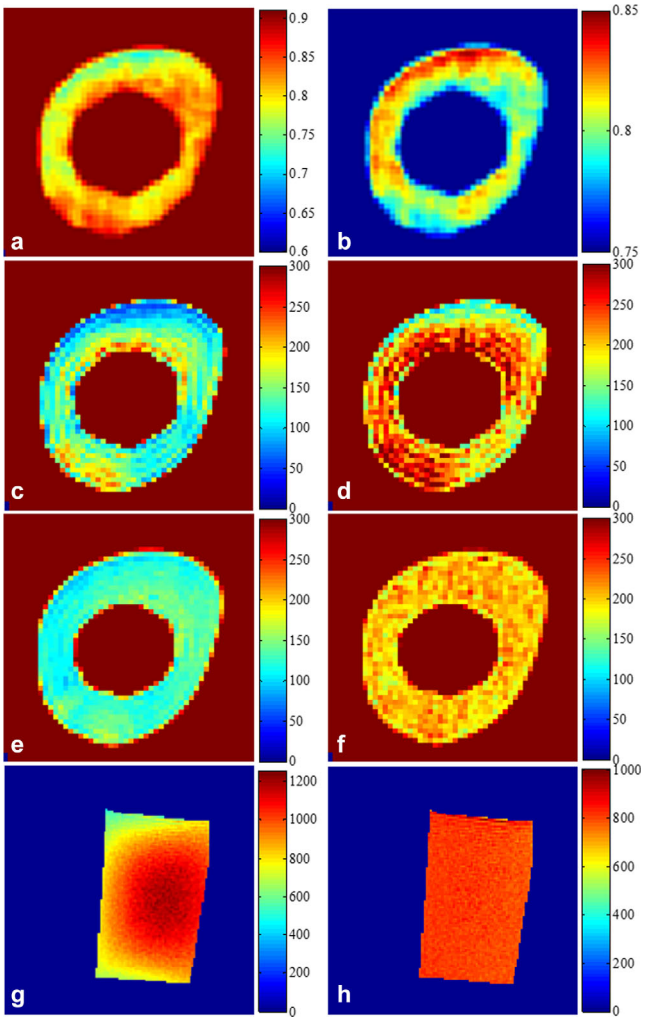

FIG. 5. Phantom T_1-related maps using 3D UTE-Cones VFA- and VTR-based methods. Cropped B_{1s} and f_z maps from the bone region of the agarose bone phantom are shown in (**a**) and (**b**). (These agarose bone phantom maps are also shown in Figs. 4g and 4h with different scaling). Panels (**c**) through (**f**) are bone T_1 maps (in units of ms) obtained using VFA without B_1 correction (**c**), VFA with B_1 correction (**d**), VTR without B_1 correction (**e**), and the proposed AFI-VTR method (**f**). The bottom row shows the T_1 maps of the agarose phantom corresponding to B_{1s} and f_z maps of the agarose phantom shown in Figures 4a to 4d, without B_1 correction (**g**) and with B_1 correction (**h**). The maps are most uniform in (**f**) and (**h**) when the AFI-VTR method is used.

with the proposed UTE-Cones AFI-VTR method is far more uniform than the T_1 map measured with the B_1-corrected VFA method or the B_1-uncorrected VTR method. For the long T_2 agarose phantom, the T_1 map obtained with the UTE-Cones AFI-VTR method was much more uniform than the T_1 map measured with the B_1-uncorrected VTR method. These results demonstrate that the proposed UTE-Cones AFI-VTR method can obtain consistent T_1 measurements for both short and long T_2 tissues.

Figure 6 shows the effect of RF pulse duration on bovine cortical bone T_1 measurement using the regular VTR and AFI-VTR methods. The bovine cortical bone T_1 measurements were obtained from the UTE-Cones VTR method with an excitation pulse of 45° and duration of 150 μs (Figs. 6e and 6f), and with an excitation pulse of 20° and duration of 60 μs (Fig. 6g) (5). As shown in Figures 6e and 6g, the T_1 map measured with the conventional B_1-uncorrected VTR method shows a higher average T_1 value when using a shorter excitation pulse (60 versus 150 μs), because of its higher excitation efficiency. Figure 6f is the same T_1 measurement as Figure 6e, but displayed with a narrower color bar range for better comparison with Figure 6g. The same color distribution can be found in Figures 6f and 6g, which suggests that they were subject to the same B_1 inhomogeneity modulation. These results demonstrate that T_1 measurements using a longer RF pulse with a lower excitation efficiency underestimate T_1 values without affecting the

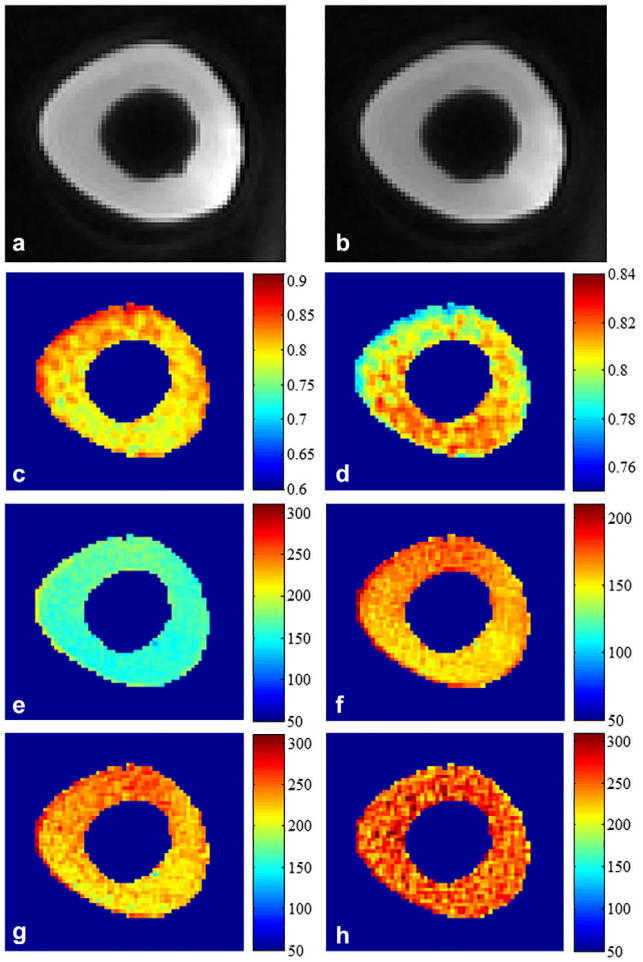

FIG. 6. The effect of RF pulse duration on bovine cortical bone T_1 measurement using the VTR method. A longer rectangular RF pulse duration of 150 μs with a flip angle of 45° was used in (**a**) to (**f**). **a, b**: Cropped sections from the 3D UTE-Cones AFI images with a TR of 20 ms (**a**) and a TR of 100 ms (**b**). The B_{1s} map (**c**) and the f_z map (**d**) were calculated from these dual TR images. **e, f**: T_1 maps obtained using the regular VTR method. The panels display a different color range. **g**: T_1 map generated with the regular VTR method using a shorter RF pulse of 60 μs and flip angle of 20°. This shows increased T_1 values relative to (**e**), but a similar T_1 spatial distribution similar to (**f**). **h**: T_1 map obtained by the 3D UTE-Cones AFI-VTR method. This shows a much more homogeneous T_1 distribution.

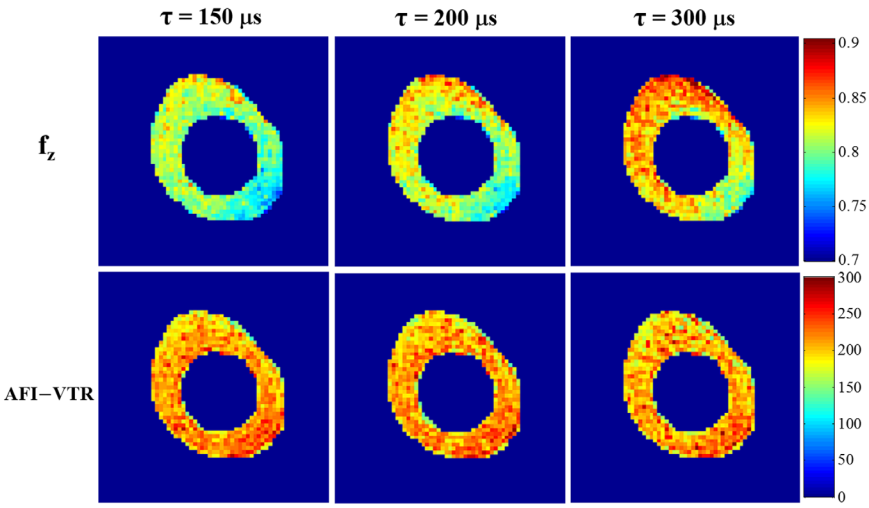

FIG. 7. Effect of RF pulse durations ($\tau = 150$, 200, and 300 μs) with the same flip angle of 45° on bovine cortical bone T_1 maps using the proposed 3D UTE-Cones AFI-VTR method. The first row shows f_z maps generated with the 3D UTE-Cones AFI method. The second row shows the 3D UTE-Cones AFI-VTR T_1 maps. These maps are uniform and consistent across each of the three RF pulse durations.

B_1 inhomogeneity modulation. Figure 6h shows the T_1 map measured with the proposed UTE-Cones AFI-VTR method, which is more uniform than that shown in Figure 6g, demonstrating that the proposed UTE-Cones AFI-VTR T_1 measurement method can correct for the effect of both B_1 inhomogeneity and excitation inefficiency.

Figure 7 further demonstrates the robustness of the proposed UTE-Cones AFI-VTR method for T_1 measurement of bovine cortical bone using rectangular RF excitation pulses with three different durations of 150, 200, and 300 μs. The mapping $f_z(\alpha, \tau, T_2)$ values increases with longer RF duration, which is consistent with the simulation results in Figure 2. However, the measured T_1 maps are almost identical, showing that the UTE-Cones AFI-VTR method can provide accurate T_1 measurement of short T_2 tissues with different excitation pulse durations.

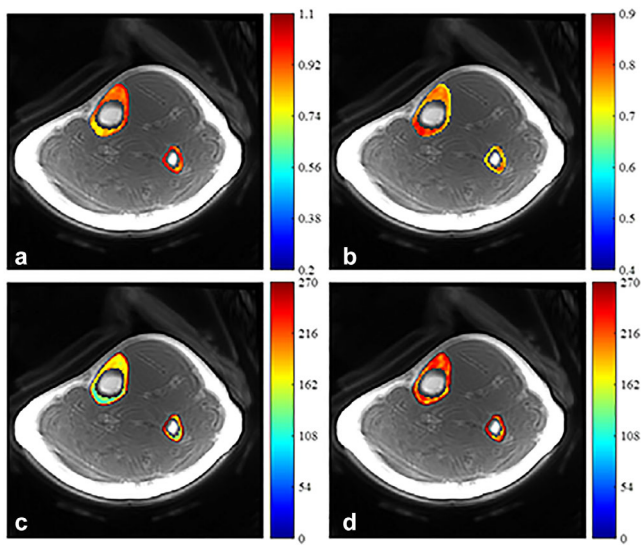

FIG. 8. In vivo tibial cortical bone results. **a, b**: B_{1s} and f_z maps calculated from 3D UTE-Cones dual-TR images, respectively. **c, d**: T_1 maps generated using the uncorrected VTR method (**c**) and using the proposed UTE-Cones AFI-VTR method (**d**), respectively. The T_1 map appears more uniform in (**d**).

Figure 8 shows in vivo T_1 mapping of the tibial midshaft in a healthy volunteer. The VTR T_1 map without correction shows lower T_1 values and more B_1 spatial modulation than the T_1 map generated with the proposed UTE-Cones AFI-VTR method, which is consistent with the simulation and phantom results.

Table 2 summarizes T_1 measurements for the bovine cortical bone samples ($N = 6$) and tibial midshaft cortical bone in the healthy volunteers ($N = 3$). The mean T_1 value and standard deviation obtained with the proposed 3D UTE-Cones AFI-VTR method for the six bovine cortical bone samples and the three in vivo human volunteer tibial cortical bones were 240 ± 25 and 218 ±± 10 ms, respectively.

DICUSSION

We have demonstrated that the proposed 3D UTE-Cones AFI-VTR method can quantify the T_1s of short T_2 tissues more accurately by dealing with the problems created by RF excitation inefficiency and B_1 inhomogeneity. Numerical simulations show that T_1 measurements using the B_1-uncorrected VTR and VFA methods are subject to errors from both B_1 inhomogeneity and excitation inefficiency. The B_1 maps obtained from Equations [7] and [8] are no longer accurate because of the complex relationship between the flip angle and the mapping functions shown in Equations [3] and [4] when imaging short T_2 species, as a result of the significant transverse magnetization loss during the relatively long RF excitation process. Simulation shows that the proposed 3D UTE-Cones AFI-VTR method provides accurate T_1 measurements for tissues with a wide range of T_2 values. The technique is relatively insensitive to the duration of the excitation pulse. Phantom and sample studies demonstrate that the 3D UTE-Cones AFI-VTR method generates uniform T_1 maps for both short (i.e., bovine cortical bone) and long (i.e., agarose phantom) T_2 tissues. In addition, the bovine cortical bone T_1 maps are nearly identical with the three different RF durations (Fig. 7), demonstrating the robustness of the proposed method. Finally, uniform T_1 maps were obtained using the proposed method to provide in

Table 2
T_1 Values and the Fitting Standard Error (in ms) Obtained by the Proposed 3D UTE-Cones AFI-VTR Method for In Vitro Bovine Cortical Bone Samples ($N = 6$) and In Vivo Human Tibial Midshaft Cortical Bone in Healthy Volunteers ($N = 3$)

In vitro bovine cortical bone sample	#1	#2	#3	#4	#5	#6
	257 ± 7	251 ± 6	211 ± 5	206 ± 8	256 ± 6	259 ± 7
In vivo human tibial cortical bone	#1		#2		#3	
	229 ± 12		215 ± 11		209 ± 9	

vivo tibial cortical bone measurements in healthy volunteers.

Many T_1 measurement techniques have been proposed including inversion recovery, saturation recovery, and SPGR-based VFA and VTR methods (32–34). The inversion-recovery method is generally regarded as the gold standard for T_1 mapping of long T_2 tissues (32). However, this inversion-recovery method is not useful for T_1 measurement of short T_2 tissues, because the typical inversion pulse available on clinical scanners is too long to provide complete inversion of the short T_2 magnetization. The saturation-recovery method provides accurate and precise T_1 measurements for short T_2 tissues (34); however, this technique is often too slow to be used clinically. SPGR-based VFA or VTR methods can provide fast volumetric T_1 mapping (4,5,19), but they suffer from high sensitivity to B_1 inhomogeneity (16–21). Obtaining an accurate B_1 map is crucial with VFA and VTR T_1 measurement approaches. Actual flip angle imaging is a fast 3D B_1 mapping technique that fits very well with VFA and VTR based T_1 corrections. It has been used for volumetric B_1 mapping of brain, body, and musculoskeletal tissues (15,20,21,35). Uniform T_1 maps can be derived using the B_1 correction. Kobayashi proposed a B_1 mapping method for short T_2s based on an implementation of the AFI technique using a 3D radial sequence called concurrent dephasing and excitation (CODE) on a 9.4T 31-cm-bore MRI system (18). The sequence shows potential for in vivo imaging on clinical scanners. Han et al proposed a 3D radial-UTE-based AFI approach for B_1 mapping of cortical bone (19). However, this group did not consider the B_1 measurement errors induced by the imperfect excitation resulting from the use of a 200-μs rectangular pulse, which could produce discontinuities in the B_1 maps at the bone-marrow boundary (19).

In contrast to these studies, our method does not require B_1 maps for T_1 correction. Instead, the longitudinal magnetization mapping function $f_z(\alpha, \tau, T_2)$ of the excitation pulse is obtained by the 3D UTE-Cones AFI method, which effectively reduces the effect of B_1 inhomogeneity. When identical RF pulses and flip angles are used with both the UTE-Cones AFI and UTE-Cones VTR sequences, the derived $f_z(\alpha, \tau, T_2)$ can be substituted in the VTR function directly for T_1 fitting. This method avoids the complex B_1 estimation from Equation [4] and corrects for both B_1 inhomogeneity and excitation inefficiency simultaneously.

As shown in the original VFA images of the agarose bone phantom (Supporting Fig. S1), ringing artifacts were present in the bone regions as a result of the relatively low image resolution used and high signal intensity difference between bone and agarose. The ringing artifacts then transferred to the calculated VFA T_1 maps (Figs. 5c and 5d). The VFA T_1 map with B_{1s} correction has a higher average T_1 value than the uncorrected VFA T_1 map. However, the spatial B_{1s} variation (Fig. 5a) still existed in the corrected VFA T_1 map (Fig. 5d) because of the inaccurate B_{1s} map that was used, and the complicated relationships between the excitation flip angles in the VFA sequences and mapping functions (Eqs. [3] and [4]). Therefore, the VFA T_1 maps did not show much improvement after B_1 correction, which was similar to the simulation results in Figure 3.

The proposed UTE-Cones AFI-VTR method could be used to measure T_1 in a variety of short T_2 tissues, including ligaments, menisci, the deep layers of articular cartilage, and myelin. In the case of myelin, the proposed 3D UTE-Cones AFI-VTR method may be used to accurately measure myelin T_1 with an extra inversion-recovery pulse to suppress signals from the long T_2 water components (36). Accurate T_1 measurements may also be crucial as input for other quantitative MRI techniques such as quantitative magnetization transfer modeling and UTE-Cones $T_{1\rho}$ imaging. These produce tissue-characterizing parameters such as macromolecular proton fraction and low frequency exchange information in short T_2 tissues (37,38).

There are several limitations to this study. First, the total data acquisition time is relatively long, in part because of the selected parameters for high accuracy, high image resolution, and broad spatial coverage. A number of strategies can be used to reduce the total scan time, including decreasing the total number of TRs, using lower resolution for f_z mapping, and advanced techniques for image reconstruction. For instance, other authors have found that T_1 can be calculated from VTR data using only two different TRs (39,40), suggesting that the total scan time of the UTE-Cones VTR sequences can be reduced (four TRs were used in the in vivo portion of our study). In addition, the scan time of UTE-Cones AFI sequence can be reduced by decreasing the image resolution for f_z measurement, and acquiring fewer slices. Furthermore, the scan time may be reduced by using advanced parallel imaging and compressed sensing reconstruction (41,42). With a combination of these strategies to greatly reduce the total scan time, our proposed 3D UTE-Cones AFI-VTR method should be acceptable in clinical applications. Second, fat and chemical shift artifacts (which produce ring artifacts in 3D UTE-Cones imaging) may lead to errors in T_1 estimation, necessitating some form of fat-water signal separation to improve accuracy (43). Third, the clinical application of the 3D UTE-Cones AFI-VTR method remains to be investigated. However, considering the importance of accurate T_1 measurement, the new technique is expected to be useful in the diagnosis and treatment monitoring of many

diseases such as osteoporosis, osteoarthritis, and multiple sclerosis, in which short T_2 tissues or tissue components are involved in the disease process.

CONCLUSIONS

The 3D UTE-Cones AFI-VTR method provides a robust technique for the measurement of T_1 of short T_2 tissues, such as cortical bone, in acceptable scan times using a clinical 3T scanner.

REFERENCES

1. Fram EK, Herfkens RJ, Johnson GA, Glover GH, Karis JP, Shimakawa A, Perkins TG, Pelc NJ. Rapid calculation of T_1 using variable flip angle gradient refocused imaging. Magn Reson Imaging 1987;5:201–208.
2. Deoni SC, Peters TM, Rutt BK. High-resolution T_1 and T_2 mapping of the brain in a clinically acceptable time with DESPOT$_1$ and DESPOT$_2$. Magn Reson Med 2005;53:237–241.
3. Cheng HL, Wright GA. Rapid high-resolution T(1) mapping by variable flip angles: accurate and precise measurements in the presence of radiofrequency field inhomogeneity. Magn Reson Med 2006;55:566–574.
4. Du J, Bydder GM. Qualitative and quantitative ultrashort-TE MRI of cortical bone. NMR Biomed 2013;26:489–506.
5. Chen J, Chang EY, Carl M, Ma Y, Shao H, Chen B, Wu Z, Du J. Measurement of bound and pore water T_1 relaxation times in cortical bone using three-dimensional ultrashort echo time cones sequences. Magn Reson Med 2017;77:2136–2145.
6. Insko E, Bolinger L. Mapping of the radiofrequency field. J Magn Reson Ser A 1993;103:82–85.
7. Cunningham CH, Pauly JM, Nayak KS. Saturated double-angle method for rapid B_1 mapping. Magn Reson Med 2006;55:1326–1333.
8. Stollberger R, Wach P. Imaging of the active B_1 field in vivo. Magn Reson Med 1996;35:246–251.
9. Morrell GR. A phase-sensitive method of flip angle mapping. Magn Reson Med 2008;60:889–894.
10. Jiru F, Klose U. Fast 3D radiofrequency field mapping using echoplanar imaging. Magn Reson Med 2006;56:1375–1379.
11. Wang D, Zuehlsdorff S, Larson AC. Rapid 3D radiofrequency field mapping using catalyzed double-angle method. NMR Biomed 2009;22:882–890.
12. Dowell NG, Tofts PS. Fast, accurate, and precise mapping of the RF field in vivo using the 180 degrees signal null. Magn Reson Med 2007;58:622–630.
13. Chavez S, Stanisz G. A simple and fast flip angle calibration method. In Proceedings of the 17th Annual Meeting of ISMRM, Honolulu, Hawaii, USA, 2009. p 375.
14. Sacolick LI, Wiesinger F, Hancu I, Vogel MW. B_1 mapping by Bloch-Siegert shift. Magn Reson Med 2010;63:1315–1322.
15. Yarnykh VL. Actual flip-angle imaging in the pulsed steady state: a method for rapid three-dimensional mapping of the transmitted radiofrequency field. Magn Reson Med 2007;57:192–200.
16. Deoni SC. High-resolution T_1 mapping of the brain at 3T with driven equilibrium single pulse observation of T_1 with high-speed incorporation of RF field inhomogeneities (DESPOT$_1$-HIFI). J Magn Reson Imaging 2007;26:1106–1111.
17. Yarnykh VL. Optimal radiofrequency and gradient spoiling for improved accuracy of T_1 and B_1 measurements using fast steady-state techniques. Magn Reson Med 2010;63:1610–1626.
18. Kobayashi N, Garwood M. B_1 mapping of short T_2* spins using a 3D radial gradient echo sequence. Magn Reson Med 2014;71:1689–1699.
19. Han M, Larson PEZ, Krug R, Rieke V. Actual flip angle imaging to improve T_1 measurement for short T_2 tissues. In Proceedings of the 23rd Annual Meeting of ISMRM, Toronto, Canada, 2015. p. 501.
20. Sinclair CD, Samson RS, Thomas DL, Weiskopf N, Lutti A, Thornton JS, Golay X. Quantitative magnetization transfer in in vivo healthy human skeletal muscle at 3 T. Magn Reson Med 2010;64:1739–1748.
21. Baudrexel S, Nürnberger L, Rüb U, Seifried C, Klein JC, Deller T, Steinmetz H, Deichmann R, Hilker R. Quantitative mapping of T_1 and T_2* discloses nigral and brainstem pathology in early Parkinson's disease. NeuroImage 2010;51:512–520.
22. Gatehouse PD, Bydder GM. Magnetic resonance imaging of short T_2 components in tissue. Clin Radiol 2003;58:1–19.
23. Robson MD, Gatehouse PD, Bydder M, Bydder GM. Magnetic resonance: an introduction to ultrashort TE (UTE) imaging. J Comput Assist Tomogr 2003;27:825–846.
24. Sussman MS, Pauly JM, Wright GA. Design of practical T_2-selective RF excitation (TELEX) pulses. Magn Reson Med 1998;40:890–899.
25. Du J, Carl M, Bydder M, Takahashi A, Chung CB, Bydder GM. Qualitative and quantitative ultrashort echo time (UTE) imaging of cortical bone. J Magn Reson 2010;207:304–311.
26. Carl M, Bydder M, Du J, Takahashi A, Han E. Optimization of RF excitation to maximize signal and T_2 contrast of tissues with rapid transverse relaxation. Magn Reson Med 2010;64:481–490.
27. Ma YJ, Zhu Y, Lu X, Carl M, Chang EY, Du J. Short T2 imaging using a 3D double adiabatic inversion recovery prepared ultrashort echo time cones (3D DIR-UTE-Cones) sequence. Magn Reson Med 2018;79:2555–2563.
28. Gurney PT, Hargreaves BA, Nishimura DG. Design and analysis of a practical 3D cones trajectory. Magn Reson Med 2006;55:575–582.
29. Carl M, Bydder GM, Du J. UTE imaging with simultaneous water and fat signal suppression using a time-efficient multispoke inversion recovery pulse sequence. Magn Reson Med 2016;76:577–582.
30. Hurley SA, Yarnykh VL, Johnson KM, Field AS, Alexander AL, Samsonov AA. Simultaneous variable flip angle–actual flip angle imaging method for improved accuracy and precision of three-dimensional T_1 and B_1 measurements. Magn Reson Med 2012;68:54–64.
31. Deoni SC, Rutt BK, Peters TM. Rapid combined T_1 and T_2 mapping using gradient recalled acquisition in the steady state. Magn Reson Med 2003;49:515–526.
32. Stanisz GJ, Odrobina EE, Pun J, Escaravage M, Graham SJ, Bronskill MJ, Henkelman RM. T_1, T_2 relaxation and magnetization transfer in tissue at 3T. Magn Reson Med 2005;54:507–512.
33. Stikov N, Boudreau M, Levesque IR, Tardif CL, Barral JK, Pike GB. On the accuracy of T_1 mapping: searching for common ground. Magn Reson Med 2015;73:514–522.
34. Techawiboonwong A, Song HK, Leonard MB, Wehrli FW. Cortial bone water: in vivo quantification with ultrashort echo-time MR imaging. Radiology 2008;248:824–833.
35. Boudreau M, Tardif CL, Stikov N, Sled JG, Lee W, Pike GB. B_1 mapping for bias-correction in quantitative T_1 imaging of the brain at 3T using standard pulse sequences. J Magn Reson Imaging 2017;46:1673–1682.
36. Du J, Sheth V, He Q, Carl M, Chen J, Corey-Bloom J, Bydder GM. Measurement of T_1 of the ultrashort T_2* components in white matter of the brain at 3T. PloS One 2014;9:e103296.
37. Ma YJ, Chang EY, Carl M, Du J. Quantitative magnetization transfer ultrashort echo time imaging using a time-efficient 3D multispoke Cones sequence. Magn Reson Med 2018;79:692–700.
38. Ma YJ, Carl M, Shao H, Tadros AS, Chang EY, Du J. Three-dimensional ultrashort echo time cones T1ρ (3D UTE-cones-T1ρ) imaging. NMR Biomed 2017;30:e3709.
39. Rad HS, Lam SCB, Magland JF, Ong H, Li C, Song HK, Love J, Wehrlia FW. Quantifying cortical bone water in vivo by three-dimensional ultra-short echo-time MRI. NMR Biomed 2011;24:855–864.
40. Abbasi-Rad S, Saligheh Rad H. Quantification of human cortical bone bound and free water in vivo with ultrashort echo time MR imaging: a model-based approach. Radiology 2017;283:862–872.
41. Ma YJ, Liu W, Tang X, Gao JH. Improved SENSE imaging using accurate coil sensitivity maps generated by a global magnitude-phase fitting method. Magn Reson Med 2015;74:217–224.
42. Lustig M, Donoho D, Pauly JM. Sparse MRI: the application of compressed sensing for rapid MR imaging. Magn Reson Med 2007;58:1182–1195.
43. Dimov AV, Liu Z, Spincemaille P, Prince MR, Du J, Wang Y. Bone quantitative susceptibility mapping using a chemical species–specific R2* signal model with ultrashort and conventional echo data. Magn Reson Med 2018;79:121–128.

SUPPORTING INFORMATION

Additional Supporting Information may be found in the online version of this article.

Fig. S1. Original VFA images with flip angle $\alpha = 8^\circ$ (left), 26° (middle), and 45° (right) in the agarose bone phantom study. There are ringing artifacts inside the bone region.